Magneto-acoustic Interfacial Reaction-Based Nanoparticle Synthesis: A Direct Path to Manufacturing Metal Matrix Nanocomposites

HUNTER B. HENDERSON, ORLANDO RIOS, SCOTT K. MCCALL, ZACHARY L. BRYAN, GERARD M. LUDTKA, and MICHELE V. MANUEL

This work investigates a novel nanoparticle fabrication methodology: combined reaction and acoustic cavitation abrasion of a solid in contact with a liquid. Magneto-Acoustic Mixing Technology is used to produce nanometer- to micron-sized particles by chemical and acoustic mechanisms between diamond particles and a stainless steel surface in the presence of a metallic liquid (Mg), where it is found that particle–surface interactions and cavitation generate particles more efficiently together than independently, producing unique chemistries. The individual and combined influence of sonic power and chemical reaction on particle size, volume fraction, chemistry, magnetic properties, and applicability to metal matrix nanocomposite fabrication are studied.

https://doi.org/10.1007/s11663-018-1320-x

INORGANIC nanoparticles are commonly produced by the decomposition of precursor materials, through a sol–gel process[1–3] or by pyrolysis.[4,5] These methods have proven effective, but attainable nanoparticle chemistries are limited by the availability of appropriate precursors and corresponding decomposition reactions. A more chemically flexible nanoparticle production approach is mechanical attrition of a bulk material into small particles in a "top down" approach[6] like rotary mills, but this process has inherent limitations with regard to input material. If insoluble particles are formed *in situ* within a fluid, the airborne release of particles is minimized, lessening the risk of environmental contamination[7–10] and respiratory distress,[11] while concurrently inhibiting agglomeration. The addition of cavitation to *in situ* approaches can enhance particle formation and enhance the wettability of particles.[12,13] This technique is appropriate for the fabrication of either nanoparticles alone or metal matrix nanocomposites (MMnC), which offer a number of mechanical property enhancements over monolithic materials.[14,15] A method that combines reaction-based synthesis with cavitation-mediated attrition of bulk material has the potential to open pathways to the creation of novel nanoparticle chemistries.

The present study investigates the proposed particle generation mechanism within the magneto-acoustic mixing technology (MAMT) process, which has been described and analyzed elsewhere.[16,17] Shown schematically in Figure 1(a), MAMT is a technique that actuates a harmonic mechanical response by the interaction of orthogonal alternating and static magnetic fields, producing sonic waves. In this setup, a radio frequency (RF) field induces eddy currents in a liquid metal contained within a steel crucible, heating the sample. An insulating alumina insert protects the induction coil and magnet bore from the high temperatures of the crucible. In addition to heating the sample, eddy currents interact with a large static magnetic field to produce an alternating Lorentz force in the crucible wall and nearby liquid. This force supplies cylindrical sinusoidal sonication to the contained sample at the induction frequency. Thermal and magnetic profiles of the MAMT process is shown in Figure 1(b), with a ramp-up of both the

HUNTER B. HENDERSON, ORLANDO RIOS, and GERARD M. LUDTKA are with the Oak Ridge National Laboratory, 1 Bethel Valley Road, Oak Ridge, TN 37830. SCOTT K. MCCALL is with the Lawrence Livermore National Laboratory, 7000 East Avenue, Livermore, CA 94550. ZACHARY L. BRYAN and MICHELE V. MANUEL are with the University of Florida, 100 Rhines Hall, 549 Gale Lemerand Drive, PO Box 116400, Gainesville, FL 32611. Contact e-mail: mmanuel@mse.ufl.edu

Manuscript submitted March 7, 2017.
Article published online August 10, 2018.

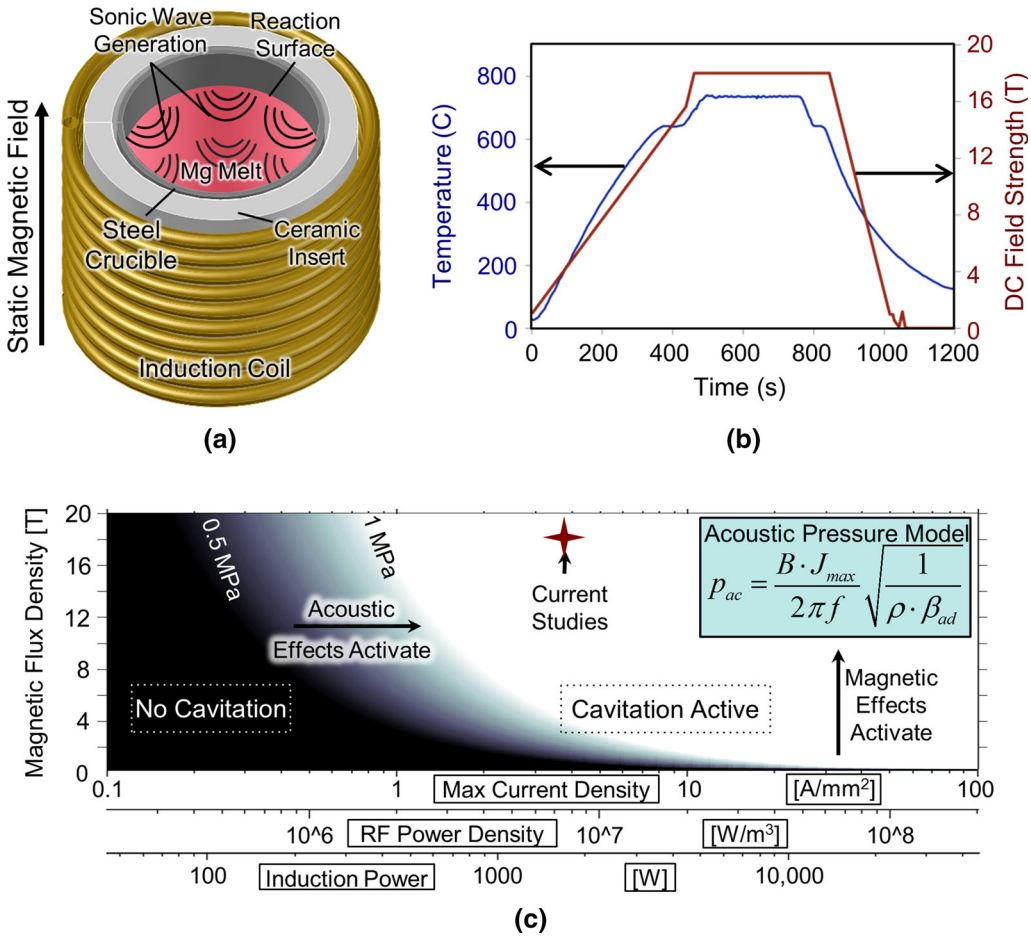

Fig. 1—(*a*) Schematic of the MAMT process showing the cylindrical nature of acoustic production and the reaction surface on the interior of the crucible. (*b*) Temperature and static magnetic field profile of the MAMT process. (*c*) Dependence of cavitation activation on magnetic field strength and induction current density, based on previous modeling of MAMT and estimates of cavitation threshold for light metals.[17] The proportionality to induction power and RF power density scales are for the current experimental geometry.

magnetic field and the sample temperature, hold at the processing temperature for 5 minutes, and a gas quench to cool. In this case, magnetic field is ramped up with temperature because the experiment took place in a Bitter magnet, but a superconducting magnet would likely be held in persistent mode. Thermal arrests at ~ 923 K (650 °C) are representative of melting and solidification. With a static magnetic flux density of 18T, acoustic intensities of 85 W/cm^2 can be achieved near the container wall, which increase as acoustic waves propagate toward the centerline of the crucible by geometric amplification.[16] The cavitation threshold for light metals is estimated to be in the range of 0.5 to 1.0 MPa,[18,19] and thus, the entire melt should undergo cavitation. The influence of processing conditions on cavitation activation (based on previous analytical modeling and the estimated cavitation threshold range of 0.5 to 1.0 MPa) is shown in Figure 1(c), with sound pressure as a function of induction current density and magnetic field strength.[16,17] In the figure, white represents the cavitation region, black the noncavitation region, and the gradient is the cavitation threshold. In the model for acoustic pressure, B is magnetic flux density, J_{max} is maximum current density, f is induction frequency, and ρ and β_{ad} are the density and the adiabatic compressibility of the liquid, respectively. It can be seen that a large magnetic field and high induction current density are required for cavitation. The other axes with induction power and RF power density (power divided by the coil volume) illustrate the current experimental setup. Proportionality between horizontal axes is a function of geometry, materials, and frequency. This technology can be adapted to an interfacial reaction-based particle generation method because the interface (the crucible sides and the melt, shown in red in Figure 1(a)) is subjected to equal acoustic intensity throughout.[16] Whereas prior studies on this precise apparatus investigated dispersion of *ex situ* particles in Mg,[20] this study aims to evaluate the possibility of producing them through an *in situ*, interfacial reaction-based mechanism.

The reaction constituents were diamond and 304 stainless steel in the presence of liquid Mg. Studies on diamond–steel interactions have shown that diamond quickly transforms to graphite in the presence of Fe at temperatures greater than 973 K (700 °C),[21,22] after which it diffuses into the steel.[23] For stainless steel, this corrosion process proceeds by pitting.[24] The reaction is

advantageous for this investigation, as pits in stainless steel can act as nucleation sites for cavitation.[25] Since cavitation can only occur in a liquid, a material that is molten at the processing temperature of 1023 K (750 °C), without participating in the reaction is desirable. Mg melts at 923 K (650 °C) and exhibits no thermodynamically favorable reactions with Fe or C,[26] so it is used as the fluid. Additionally, liquid Mg is electrically conductive, a requirement for acoustic generation by MAMT. The base materials included 99.8 pct Mg extruded rod (Strem Chemical) and 50 nm aqueous diamond (Advanced Abrasives). The crucibles were produced by attaching 2 mm thick 304 stainless steel tubing and sheet by laser welding with no filler. Both materials were supplied by McMaster Carr and meet ASTM A269. The diamond particles were dried on a hot plate and manually crushed prior to other processing. The samples were preprocessed by melting the magnesium rod in the stainless steel crucible under argon and casting around a thermocouple sleeve composed of stainless steel. Holes were drilled into the solidified Mg, which was filled with 1 vol. pct diamond nanoparticles and capped with 99.99 pct Mg slugs (Alfa Aesar).

Processing took place at the National High Magnetic Field Laboratory, Tallahassee, FL, in a 20 T, 195 mm bore resistive Bitter magnet operated at 18 T. A customized setup, which included crucible support, alumina insulation, an induction coil, and argon and helium flow, was used inside the bore of the magnet to apply MAMT power. The processing steps were as follows. First, the induction coil heated the sample in the crucible under an argon atmosphere, while the static magnet ramped-up to 18 T. The sample melted and reached a processing temperature of 1000 K (727 °C), where it received 2.8 kW of induction energy at 10 kHz. Thermal control during a 5 minutes isothermal hold was maintained by mixing helium with the argon. Calculations indicate that the crucible wall was under an acoustic pressure of 2200 kPa. Helium flow was increased to cool the sample, and the induction heater is switched off 20 K (20 °C) prior to solidification.

Three samples were investigated: P (50-nm diamond "particle" reactants with no acoustic treatment), S ("sonic" treatment only), and SP ("sonic" treatment with diamond "particle" reactants). Samples P and SP contained 1 vol. pct of the diamond as seen in Figures 2(a) and (b). Sample P underwent induction melting similar to samples S and SP, but with no static magnetic field to eliminate acoustic effects.

Optical tomography images of solidified microstructures were obtained using a Leica DM2500. Transmission electron microscopy (TEM) was performed on a JEOL 200cx operating at 200 kV. Standard focused ion beam (FIB) cross-sectional techniques were used to prepare the samples for TEM.

Magnetic measurements were performed in a Quantum Design MPMS-5 SQUID magnetometer using right cylindrical samples with masses in the range of 40 to 65 mg. At low temperatures, the sample was held in a polypropylene straw. $M(T)$ measurements were made at several applied fields (0.1, 0.5, 1 kOe), and isothermal $M(H)$ measurements were made for several

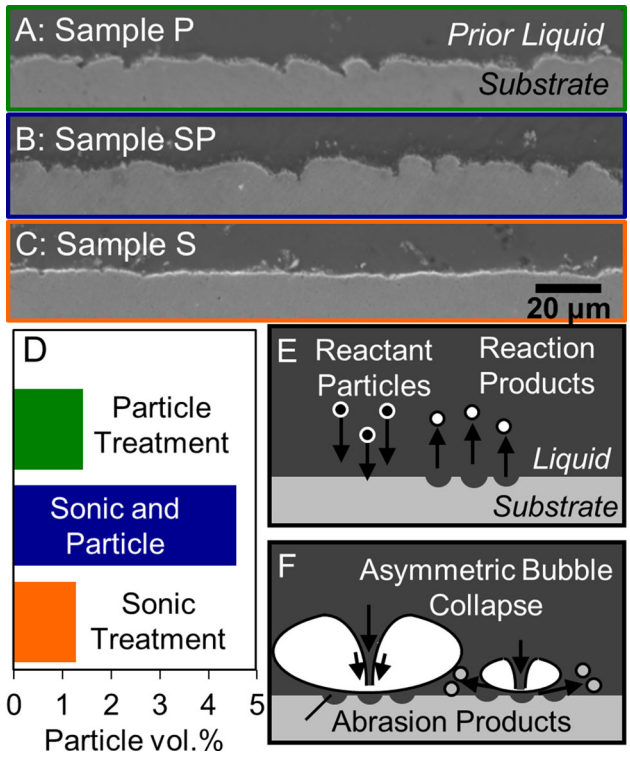

Fig. 2—Cross-sectional substrate morphologies of (*a*) Sample P, (*b*) Sample SP, and (*c*) Sample S. P and S received particle or sonic treatment, respectively, while SP received both sonic energy and particles. Schematics of (*e*) surface/particle chemical reaction and (*f*) microjet abrasion. (*d*) Volume percentages of particles in the samples.

temperatures. Measurements from 300 K to 750 K (27 °C to 477 °C) were obtained with smaller samples (5 to 15 mg) using an oven insert and custom-designed brass tube with quartz spacers.

The postprocessing crucible–melt interfacial roughness is shown in Figures 2(a) through (c). The samples that contained diamond (P and SP) both exhibited a pitted interface, while the sample that underwent sonic treatment (Sample S) was relatively smooth. As mentioned, carbon reacts with stainless steel above 973 K (700 °C) to form reaction pits, visible in Figures 2(a) and (b). The particle volume fractions of the samples (particle sizes ranging from 1 to 50 μm measured by optical microscopy tomography) are shown in Figure 2(d). Energy dispersive X-ray spectroscopy (EDS) analysis of particles ranging from 1 to 50 μm showed that they contain varying ratios of Fe and Cr (from stainless steel), with no Ni visible. Sample SP contained three times as many particles in this range as either Sample S or P, implying that particle generation is more effective when both sonic and particle treatment are active than it is with only one type of treatment.

These particles are hypothesized to be produced by two combinatorial mechanisms, as shown in Figures 2(e) and (f). As reactant particles impinge on the surface and form reaction products, they leave reaction pits and a rough surface. This roughness provides nucleation sites for cavitation bubbles,[25] which collapse asymmetrically when near a surface,

subjecting the surface to a jet of high-speed liquid in a process called microjet formation. This liquid can cause additional abrasion of the surface, and peaks on the surface act as easy sites for particle generation in this mechanism. Unfocused cavitation, like that expected in MAMT, has been shown to evenly polish surfaces.[27] These processes may be complementary, as pits formed by reacting particles will increase particle generation by cavitation, leaving smooth surfaces for further particle reaction.

The distribution of particles in the solidified samples was further studied with magnetometry and TEM. Magnetization data at 300 K (27 °C) for unprocessed pure Mg and three particle-containing samples is shown in Figure 3(a). The pure Mg had a linear magnetic susceptibility, $\chi = M/H$,[28] at 300 K (27 °C) of 1.28×10^{-5}, slightly higher than expected for pure Mg (1.13×10^{-5}),[29] and $\chi(T)$ showed a low-temperature Curie tail consistent with < 100 ppm local moment impurities (*e.g.* Fe, Co, Ni). 304 stainless steel is austenitic and paramagnetic with a linear magnetic susceptibility of the order of 3×10^{-3}.[30] However, work hardening can induce partial transformation to martensite, which is magnetically ordered.[28] The samples consist of a mélange of particles varying in size and chemistry, so a complete quantitative analysis is not possible because of multiple competing phenomena. However, comparative analysis permits some insight. All three of the sample treatments show Langevin behavior that persists to above 600 K (327 °C) and indicates ferromagnetism. For α-Fe, the saturation moment is 220 Am^2/kg,[31] while the volume-normalized moments are 0.78, 0.87, and 0.23 Am^2/kg for the S, P, and SP samples, respectively. This corresponds to a ferromagnetic contribution of less than one percent of the particle volume, implying the majority of the large steel particles remain austenitic.

Figure 3(b) shows $\chi(T)$ measured at 1 kOe for the four materials. The particle-containing samples have far larger values than the pure Mg sample, with several observable features. Both samples with added diamond particles (P, SP) display a broad shoulder between 300 K and 500 K (27 °C to 227 °C), while the S sample shows no similar feature. Cementite (Fe_3C) ferromagnetically orders at 481 K and addition of Cr depresses this value.[32] Thus, the shoulders observable in the $\chi(T)$ data suggest a reaction between the diamond and steel particles to form small amounts of $(Fe,Cr)_3C$.

An interesting result arises in samples treated with MAMT—the zero-feld-cooled $\chi(T)$ curves measured at

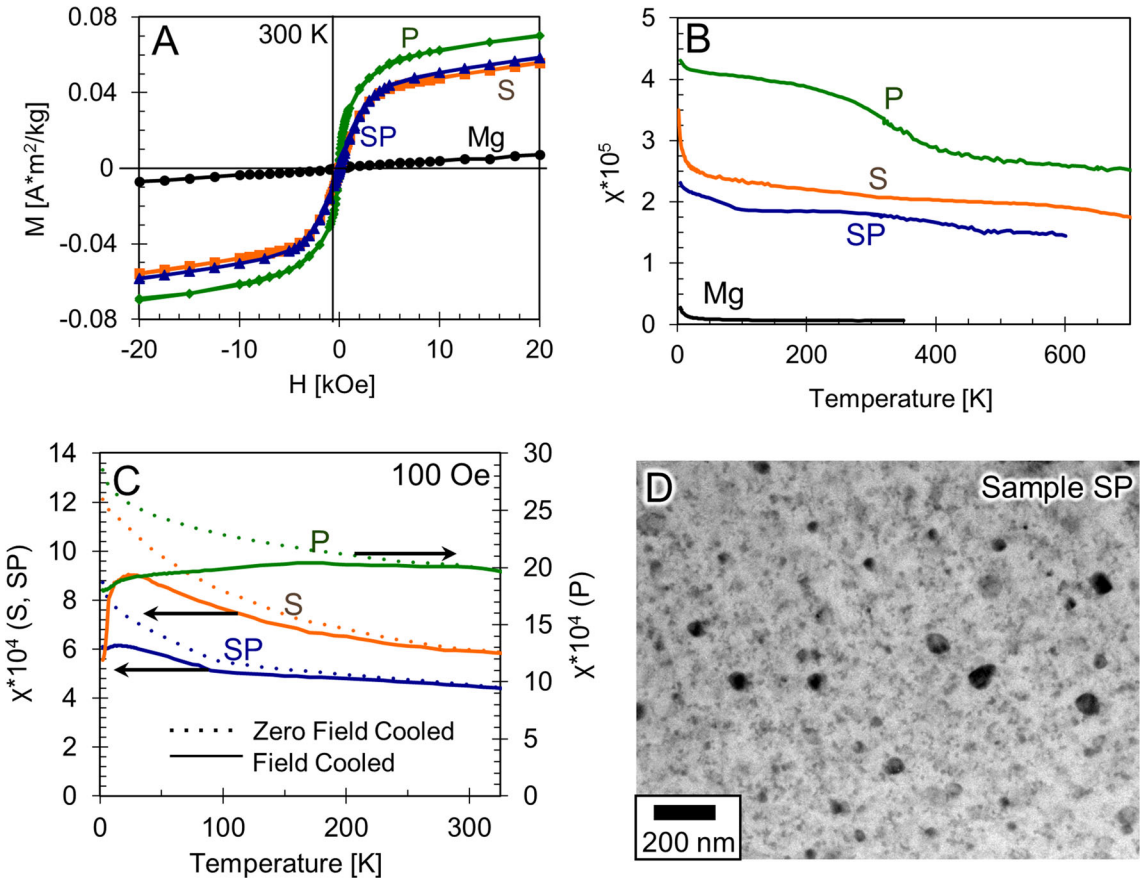

Fig. 3—(*a*) Magnetization of Mg starting material and particle containing samples, the latter of which fit well to a Langevin function, a signature of ferromagnetism, and linear term. Evaluation of the moment as a function of particle volume indicates less than 0.5 pct of the particles are ferromagnetic. (*b*) Magnetization at 1 kOe. The broad shoulders of the P and SP samples suggest the presence of cementite-based alloys $(Fe,Cr)_3C$. (*c*) Field-Cooled and Zero Field-Cooled data for SP, S, and P in 100 Oe. Evidence of superparamagnetism can be seen in Samples S and SP. (*d*) TEM brightfield image of a group of particles in Sample SP.

100 Oe (Figure 3(c)) show peaks suggesting significant numbers of superparamagnetic particles. Superparamagnetism occurs when the magnetic energy of a nanoparticle is comparable to its thermal energy (k_BT), and it undergoes spontaneous magnetic reorientation. The particles will appear magnetically stable when the average time between reiorientations is large relative to the measurement time. For a given particle size, this temperature is known as the blocking temperature and occurs as a peak in the zero-feld-cooled data as observed for the samples subjected to MAMT, but not for the diamond particles only. The peaks arise at 25 K (− 248 °C) for sample S and 15 K (− 258 °C) for sample SP which correspond to diameters of 10 and 8.8 nm, respectively. This assumes spherical particles consisting primarily of α-Fe, with the first anisotropy constant: $K_1 = 5.84 \times 10^4$ J/m^3 at 4.2 K (− 269 °C)[33] and taking $K = K_1/4$ for a cubic system. The SP result is consistent with observations of particle size by TEM, shown in Figure 3(d). In each case, the peaks show a broad roll-off with increasing temperature consistent with a distribution of larger particle sizes. For sample SP, there is a distinct change in slope around 90 K (− 183 °C), suggesting a sharp decrease in the number of magnetic nanoparticles beyond ~ 15 nm and may indicate that MAMT preferentially produces nanoparticles with magnetic character, in addition to the micron-scale abrasion products.

In conclusion, a combinatorial reaction/cavitation mechanism has been proposed by which particles create surface pits, which are targeted by cavitation microjet abrasion to generate particles. In the current study, an MAMT system has been shown to create particles with a wide range of sizes from a reaction of diamond and stainless steel in the presence of liquid Mg. Based on magnetometry, partial transformation of the austenitic starting material to ferromagnetic particles occurred in all samples, but was greatly enhanced by diamond particles. These particles reacted to form $(Fe,Cr)_3C$ and superparamagnetic nanoparticles. This approach can be used to produce MMnCs directly by an *in situ* method, leading to nonagglomerated composites. More study is required to control the chemistry and size of particles in this system. Future studies can also focus on expanding the range of particle chemistries that can be produced by this method, expanding on the fundamental generation mechanisms for adequate input down selection. Furthermore, based on Figure 1(c), cavitation should be active at a lower field of 9T, meaning that more economic and scalable superconducting magnets could be used for this. Regardless, the current method has the potential to fabricate particles with chemistries far from equilibrium, potentially not available from other techniques.

ACKNOWLEDGMENTS

The authors wish to thank the National High Magnetic Field Laboratory, Tallahassee, FL, for allowing the generous use of their DC magnet facilities, and the Manufacturing Demonstration Facility at the Oak Ridge National Laboratory for providing sample handling and electromagnetic processing apparatus. This article is based upon work supported by the National Science Foundation under grant number DMR-0845868, sponsored in part by the Critical Materials Institute, an Energy Innovation Hub funded by the U.S. Department of Energy, Office of Energy Efficiency and Renewable Energy, Advanced Manufacturing Office, under DE-AC05-00OR22725 with UT-Battelle, LLC. Work done at LLNL was prepared under Contract DE-AC52-07NA27344. The authors would also like to thank the Major Analytical Instrumentation Center at the University of Florida.

OPEN ACCESS

ELECTRONIC SUPPLEMENTARY MATERIAL

The online version of this article (https://doi.org/10.1007/s11663-018-1320-x) contains supplementary material, which is available to authorized users.

REFERENCES

1. F. Zaera: *Chem. Soc. Rev.*, 2013, vol. 42, pp. 2746–62.
2. M.A. Faramarzi and A. Sadighi: *Adv. Colloid Interface Sci.*, 2013, vol. 189, pp. 1–20.
3. H. Bazrafshan, Z. Alipour Tesieh, S. Dabirnia, and A. Naderifar: *Mater. Manuf. Process.*, 2016, vol. 31, pp. 119–25.
4. A.J. Grohn, S.E. Pratsinis, A. Sanchez-Ferrer, R. Mezzenga, and K. Wegner: *Indust. Eng. Chem. Res.*, 2014, vol. 53, pp. 10734–42.
5. O. Arutanti, A.B.D. Nandiyanto, T. Ogi, F. Iskandar, T.O. Kim, and K. Okuyama: *J. Alloys Compd.*, 2014, vol. 591, pp. 121–26.
6. C.L. De Castro and B.S. Michell: *Nanoparticles from Mechanical Attrition*, American Scientific Publishers, Stevenson Ranch, 2003.
7. M.A. Zoroddu, S. Medici, A. Ledda, V.M. Nurchi, J.I. Lachowicz, and M. Peana: *Curr. Med. Chem.*, 2014, vol. 21, pp. 3837–53.
8. S.C.N. Tang and I.M.C. Lo: *Water Res.*, 2013, vol. 47, pp. 2613–32.
9. Z. Magdolenova, A. Collins, A. Kumar, A. Dhawan, V. Stone, and M. Dusinska: *Nanotoxicology*, 2014, vol. 8, pp. 233–78.
10. R.A. Yokel, S. Hussain, S. Garantziotis, P. Demokritou, V. Castranova, and F.R. Cassee: *Environ. Sci.*, 2014, vol. 1, p. 406.
11. C. Medina, M.J. Santos-Martinez, A. Radomski, O.I. Corrigan, and M.W. Radomski: *Br. J. Pharmacol.*, 2007, vol. 150, pp. 552–58.
12. K.S. Suslick, Y. Didenko, M.M. Fang, T. Hyeon, K.J. Kolbeck, W.B. McNamara, M.M. Mdleleni, and M. Wong: *Philos. Trans. R. Soc. Lond. A*, 1999, vol. 357, pp. 335–53.
13. J.H. Bang and K.S. Suslick: *Adv. Mater.*, 2010, vol. 22, pp. 1039–59.
14. Song.-Jeng. Huang, Po.-Chou. Lin, and Jong.-Ning. Aoh: *Mater. Manuf. Process.*, 2015, vol. 30, pp. 1272–77.
15. J.B. Ferguson, F. Sheykh-Jaberi, C.S. Kim, P.K. Rohatgi, and K. Cho: *Mater. Sci. Eng. A*, 2012, vol. 558, pp. 193–204.

16. H.B. Henderson, O. Rios, Z.L. Bryan, C.P. Heitman, G.M. Ludtka, G. Mackiewicz-Ludka, A.M. Melin, and M.V. Manuel: *Adv. Eng. Mater.*, 2014, vol. 16, pp. 1076–82.
17. H.B. Henderson, O. Rios, G.M. Ludtka, and M.V. Manuel: *Metall. Mater. Trans. B*, 2015, vol. 46, pp. 2020–27.
18. G.I. Eskin: *Ultrasonic Treatment of Light Alloy Melts*, Gordon and Breach Science Publishers, Amsterdam, 1998.
19. G.I. Eskin: *Ultrasonics Sonochem.*, 1995, vol. 2, pp. S137–41.
20. H.B. Henderson, O. Rios, Z.L. Bryan, C.P.K. Heitman, G.M. Ludtka, G. Mackiewicz-Ludtka, A.M. Melin, and M.V. Manuel: *Adv. Eng. Mater.*, 2014, vol. 16, pp. 1078–82.
21. A.G. Thornton and J. Wilks: *Nature*, 1978, vol. 274, pp. 792–93.
22. Y.C. Song, K. Nezu, C.H. Park, and T. Moriwaki: *Int. J. Mach. Tools Manuf.*, 2009, vol. 49, pp. 339–43.
23. R. Narulkar, S. Bukkapatnam, L.M. Raff, and R. Komanduri: *Comput. Mater. Sci.*, 2009, vol. 45, pp. 358–66.
24. N.G. Thompson, R.A. Buchanan, and J.E. Lemons: *J. Biomed. Mater. Res.*, 1979, vol. 13, pp. 35–44.
25. J.P. Nail, R.I. Vachon, and J. Morehouse: *J. Heat Transfer.*, 1974, vol. 96, pp. 132–37.
26. M. Binnewies and E. Milke: *Thermochemical Data of Elements and Compounds*, Wiley-VCH, Weinheim, 2002.
27. H. Yamaguchi, T. Shinmura, K. Kasai, and T. Aizawa: *Trans. Jpn. Soc. Mech. Eng. Ser. C*, 2002, vol. 68, pp. 2777–82.
28. K.H. Lo, C.H. Shek, and J.K.L. Lai: *Mater. Sci. Eng. R*, 2009, vol. 65, pp. 39–104.
29. H.U. Åström and K. Svensson: *Phys. Scr.*, 1970, vol. 1, p. 66.
30. T. Kobayashi, S. Kobayashi, K. Itoh, and K. Tsuchiya: *AIP Conf. Proc.*, 2002, vol. 614, pp. 92–96.
31. H. Kura, M. Takahashi, and T. Ogawa: *J. Phys. Chem. C*, 2010, vol. 14, pp. 5835–38.
32. M. Umemoto, Z.G. Liu, K. Masuyama, and K. Tsuchiya: *Scr. Mater.*, 2001, vol. 45, pp. 391–7.
33. W. Björn, N. Per, and N. Lars: *Phys. Scr.*, 1975, vol. 11, p. 383.